

ISSN: 0095-8972 (Print) 1029-0389 (Online) Journal homepage: <http://www.tandfonline.com/loi/gcoo20>


# Studies of the gas sorption, magnetism and luminescence on two polymers constructed from 1,3,5-benzenetribenzoate ligand

Wei-Ping Wu, Xi-Ren Wu, Lu Lu & Jun Wang


To cite this article: Wei-Ping Wu, Xi-Ren Wu, Lu Lu & Jun Wang (2015) Studies of the gas sorption, magnetism and luminescence on two polymers constructed from 1,3,5-benzenetribenzoate ligand, Journal of Coordination Chemistry, 68:1, 130-141, DOI: 10.1080/00958972.2014.981168



To link to this article: <http://dx.doi.org/10.1080/00958972.2014.981168>

 View supplementary material 


 Accepted author version posted online: 27 Oct 2014.  
Published online: 25 Nov 2014.

 Submit your article to this journal 

 Article views: 58

 View related articles 

 View Crossmark data 

 Citing articles: 1 View citing articles 

## Studies of the gas sorption, magnetism and luminescence on two polymers constructed from 1,3,5-benzenetribenzoate ligand

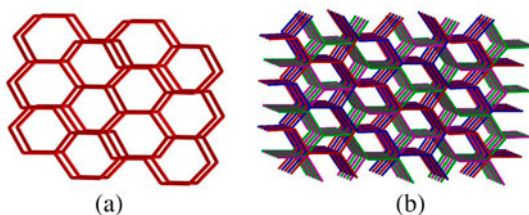
WEI-PING WU<sup>\*†‡</sup>, XI-REN WU<sup>§,1</sup>, LU LU<sup>†‡</sup> and JUN WANG<sup>\*†‡</sup>

<sup>†</sup>Institute of Functionalized Materials, Sichuan University of Science & Engineering, Zigong, PR China

<sup>‡</sup>School of Chemistry and Pharmaceutical Engineering, Sichuan University of Science & Engineering, Zigong, PR China

<sup>§</sup>School of Pharmacy, Dongguan Guangdong Medical College, Dongguan, PR China

(Received 27 June 2014; accepted 1 October 2014)



This work represents a new 4-fold interpenetrated honeycomb coordination polymer, which was also characterized by gas sorption and luminescence. The compound exhibits strong photoluminescence at room temperature and may be suitable as a candidate as a luminescent material.

Solvothermal reaction of 1,3,5-benzenetribenzoic acid ( $H_3btb$ ) with metal salts yielded two compounds with chemical formulas  $\{(Me_2NH_2)[Zn(bt b)(DMA)] \cdot DMA\}_n$  (**1**) and  $[Mn_3(bt b)_2(DMA)_4 \cdot 4DMA]$  (**2**) (DMA = N,N'-dimethylacetamide). **1** shows a 3-D fourfold interpenetrating (6,3) topological net, which has 1-D channels with counter anion and guest DMA molecules. **2** contains a 2-D bilayer structure based on a carboxylate-bridged  $Mn_3$  cluster. **1** has no significant adsorption for  $H_2$  and  $N_2$  gas upon desolvation by long-time thermal activation, indicating that access to the void space is blocked by the immovable anions and interpenetrated feature. In addition, the 3-D luminescence for **1** and magnetism for **2** were also explored.

*Keywords:* Luminescence; Gas sorption; Magnetism; Interpenetration

### Introduction

Metal-organic frameworks (MOFs) have been evaluated for their promising applications in luminescence and gas technology [1–5]. Thanks to the large variety of metal centers,

\*Corresponding authors. Email: [wuweipingzg@126.com](mailto:wuweipingzg@126.com) (W.-P. WU); [scwangjun2011@126.com](mailto:scwangjun2011@126.com) (J. Wang)

<sup>1</sup>W.-P. Wu and X.-R. Wu have equally contributed to this work and joint first authors.

commonly called nodes, and of organic bridging ligands, referred to as linkers, there is a virtually limitless possibility of combination of secondary building units that can be assembled into MOFs. This extreme diversity does however also pose challenges, both for categorizing the different classes of MOFs and for predicting which molecular architecture, or topology might form with a chosen set of nodes and linkers under specific reaction conditions [6–8].

1,3,5-Benzenetricarboxylic acid ( $H_3btb$ ) has been extensively used for construction of coordination polymers, resulting in a variety of large pore architectures with interesting properties. Many Zn-*btb* compounds have been explored [9–12]. Moreover, the formations of diverse MOFs with large pores may lead to interpenetration. As a type of entanglement, interpenetration has been the most investigated and merits of the interpenetrating networks have been discovered. Some researchers proved that interpenetration could be utilized to strengthen the interaction between the gas molecules and the frameworks. To prepare new materials with interpenetration and good physical properties, we chose *btb* as a single bridging ligand to react with the d-block metal salts and obtained two new 3-D coordination polymers,  $\{(Me_2NH_2)[Zn(btb)(DMA)] \cdot DMA\}_n$  (**1**) and  $[Mn_3(btb)_2(DMA)_4 \cdot 4DMA]$  (**2**) (DMA = N,N'-dimethylacetamide). **1** shows a 3-D fourfold interpenetrating (6,3) topological net, which represents the highest interpenetrated mode in Zn-*btb* compounds. **2** contains a 2-D bilayer structure based on a carboxylate-bridged  $Mn_3$  cluster. The gas sorption and 3-D luminescence for **1** and magnetism for **2** were explored.

## Experimental

### Materials and methods

All reagents were purchased from commercial sources and used as received. IR spectra were recorded with a PerkinElmer Spectrum One spectrometer from 4000 to 400  $cm^{-1}$  using KBr pellets. Thermogravimetric analyses (TGA) were carried out with a Mettler–Toledo TA 50 in dry dinitrogen ( $60 mL min^{-1}$ ) at a heating rate of 5  $^{\circ}C min^{-1}$ . X-ray powder diffraction (XRPD) data were recorded on a Rigaku RU200 diffractometer at 60 kV, 300 mA with Cu  $K_{\alpha}$  radiation ( $\lambda = 1.5406 \text{ \AA}$ ), with a scan speed of 2  $^{\circ}C min^{-1}$ , and a step size of 0.013 $^{\circ}$  in  $2\theta$ . Luminescence spectra for crystal solid samples were recorded at room temperature on an Edinburgh FLS920 phosphorimeter (USA). Gas sorption isotherms were measured using ASAP 2020 M adsorption equipment. Magnetic susceptibility data of powdered sample restrained in parafilm were measured on an Oxford Maglab 2000 magnetic measurement system from 300 to 1.8 K and at field of 1 kOe.

### X-ray crystallography

Single-crystal X-ray diffraction analyses of the compounds were carried out on a Bruker SMART APEX II CCD diffractometer equipped with graphite-monochromated  $MoK_{\alpha}$  radiation ( $\lambda = 0.71073 \text{ \AA}$ ) using  $\Phi/\omega$  scan technique at room temperature. The intensities were corrected for Lorentz and polarization effects as well as for empirical absorption based on multi-scan techniques; the structures were solved by direct methods and refined by full-matrix least-squares fitting on  $F^2$  using SHEXL-97 [13]. Absorption corrections were applied using the multi-scan approach with SADABS [14]. Hydrogens of the organic ligands were placed in calculated positions and refined using a riding model on attached

Table 1. Crystallographic data and structure refinement details for **1** and **2**.

Complex	<b>1</b>	<b>2</b>
Empirical formula	C <sub>37</sub> H <sub>41</sub> N <sub>3</sub> O <sub>8</sub> Zn	C <sub>86</sub> H <sub>102</sub> Mn <sub>3</sub> N <sub>8</sub> O <sub>20</sub>
Formula mass	419.08	1732.57
Crystal system	Monoclinic	Monoclinic
Space group	<i>P</i> 21/ <i>n</i>	<i>P</i> 21/ <i>n</i>
<i>a</i> [Å]	14.265(4)	12.2866(15)
<i>b</i> [Å]	8.945(2)	26.175(3)
<i>c</i> [Å]	27.441(6)	13.7252(16)
$\alpha$ [°]	90	90
$\beta$ [°]	90.451(4)	98.6324(19)
$\gamma$ [°]	90	90
<i>V</i> [Å <sup>3</sup> ]	3501.3(15)	4364.1(9)
<i>Z</i>	4	2
$\mu$ [mm <sup>-1</sup> ]	1.368	0.500
<i>F</i> (0 0 0)	1512	1818
Reflections collected	21,921	36,217
<i>R</i> <sub>(int)</sub>	0.0722	0.0624
<i>R</i> <sub>1</sub> , <i>wR</i> <sub>2</sub> [ <i>I</i> > 2 $\sigma$ ( <i>I</i> )]	0.0466, 0.0894	0.0452, 0.1014
<i>R</i> <sub>1</sub> , <i>wR</i> <sub>2</sub> [all data]	0.0905, 0.1041	0.0685, 0.1124

Table 2. Selected bond distances (Å) and angles (°) for **1** and **2**.

<b>1</b>			
Zn1–O1	1.9505(17)	Zn1–O7	2.0250(19)
Zn1–O4	1.9459(18)	Zn1–O5	1.9597(17)
O4–Zn1–O1	108.43(8)	O4–Zn1–O5	108.30(8)
O1–Zn1–O5	132.89(7)	O7–Zn1–O4	88.98(8)
O1–Zn1–O7	102.73(8)	O5–Zn1–O7	106.39(8)
<b>2</b>			
Mn1–O1	2.1172(12)	Mn1–O5	2.1396(12)
Mn1–O7	2.1457(12)	Mn1–O8	2.1774(12)
Mn1–O4	2.2721(11)	Mn1–O3	2.3105(12)
Mn2–O2#1	2.1235(12)	Mn2–O6#1	2.1271(11)
Mn2–O4#1	2.2127(11)	O1–Mn1–O5	95.95(5)
O5–Mn1–O8	169.11(5)	O7–Mn1–O4	158.98(5)
O2–Mn2–O2	180.00(7)	O6–Mn2–O6	180
O4–Mn2–O4	180	O2–Mn2–O6	84.65(5)

Note: Symmetric codes: #1:  $-x + 1/2, y + 1/2, -z + 1/2$ .

atoms with isotropic thermal parameters 1.2 times those of their carrier atoms. Table 1 shows crystallographic data of **1** and **2**. Selected bond distances and angles are listed in table 2. CCDC: 1009181 for **1** and 1004378 for **2**.

## Syntheses

**{(Me<sub>2</sub>NH<sub>2</sub>)[Zn(btbt)(DMA)]·DMA}<sub>n</sub> (1)**. A mixture of Zn(OAc)<sub>2</sub> (0.1 mM), H<sub>3</sub>btbt (0.1 mM), DMF (8 mL), and HNO<sub>3</sub> (0.1 mL) was placed in a Teflon-lined stainless steel vessel, heated to 120 °C for 3 days under autogenous pressure, and then cooled to room temperature at 5 °C h<sup>-1</sup>. Colorless crystals were obtained after 5 days. The resulting crystals formed were filtered off, washed with water, and dried in air. C<sub>37</sub>H<sub>41</sub>N<sub>3</sub>O<sub>8</sub>Zn Calcd: C, 61.62; H, 5.73; N, 5.83. Found: C, 61.40; H, 5.70; N, 5.79. IR (KBr, cm<sup>-1</sup>): 3442(vs); 3054(m); 2953(m); 1617(vs); 1352(vs); 1244(s); 1165(vs); 1018(vs); 840(vs).

**[Mn<sub>3</sub>(btb)<sub>2</sub>(DMA)<sub>4</sub>·4DMA] (2).** A mixture of Mn(OAc)<sub>2</sub>·H<sub>2</sub>O (0.1 mM), H<sub>3</sub>BTB (0.1 mM), DMA (5 mL), deionized water (1 mL), and HNO<sub>3</sub> (0.1 mM) was stirred for 30 min in air, kept at 120 °C for 3 days in an oven, and then cooled to 25 °C. The resulting crystals formed were filtered off, washed with water, and dried in air. C<sub>86</sub>H<sub>102</sub>Mn<sub>3</sub>N<sub>8</sub>O<sub>20</sub> Calcd: C, 59.62; H, 5.93; N, 6.47. Found: C, 59.45; H, 6.02; N, 6.41. IR (KBr, cm<sup>-1</sup>): 3396(m); 2922(vs); 1569(m); 1531(m); 1399(m); 1251(m); 1011(vs); 769(vs).

## Results and discussion

### $\{(Me_2NH_2)[Zn(btb)(DMA)]\cdot DMA\}_n$ (**1**)

X-ray crystallography reveals that **1** crystallizes in the space group  $P 2_1/n$ . In the asymmetric unit, each Zn(II) is four-coordinate with three oxygens from three different carboxyl groups (Zn–O 1.9543(10)–1.9620(10) Å) and one O (Zn1–O7 = 2.0252(10) Å) from coordinated DMA exhibiting a slightly distorted tetrahedral geometry (figure 1). Btb in **1** has the highest symmetry. The dihedral angle between central benzene and adjacent benzene was 4.8°, and the dihedral angle between benzene rings was 7.9°, which demonstrated that btb was essentially coplanar. The carboxylate was almost coplanar with benzene ring with a torsion angle of 4.8°. The three carboxylate groups from each btb are monocoordinated. In this crystal, the Zn(II) centers are polymerized through the btb units to yield 2D layers with large pores along the *ac*-plane. These layers are further connected by btb units, generating an interesting

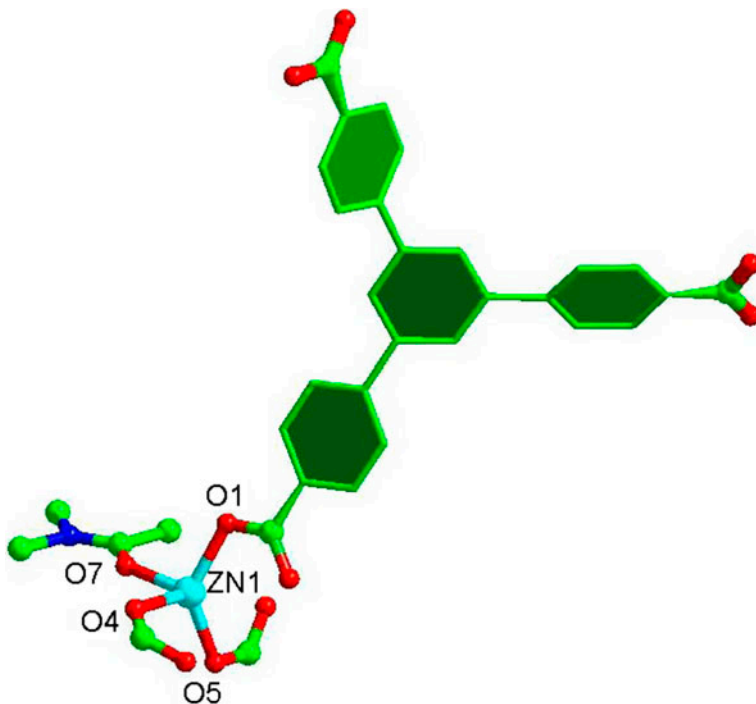


Figure 1. View of the coordination environment of Zn(II) center in **1**.

3-D framework. There also exist 1-D channels along the *b* direction (figure 2). There were hexagonal cavities in the complex. Three *btb* ligands encompassed a fully empty hexagonal cavity with a dimension of 16.8(7) Å edge distances (figure 2). The two set cavities compensated each other and arranged face-to-face to form a rotation angle of 40° instead of coinciding. The centroid-to-centroid distances of the phenyl in the adjacent parallel *btb* were 3.5 Å with  $\pi$ - $\pi$  stacking interactions between the phenyl rings. Similar to reported complexes, there was one proton in the formula to balance the charge. There exist some hydrogen bonding interactions between guest  $\text{Me}_2\text{NH}_2$  and DMA molecules (figure 2). The  $\text{Me}_2\text{NH}_2$  also binds to uncoordinated O from the carboxylate groups.

To fully understand the structure of **1**, the topological approach is applied to simplify such a 3-D coordination network. The *btb* ligand takes the 3-connected nodes to link three Zn(II) centers, and the Zn(II) also serves as the 3-connected nodes. In this way, **1** can be reduced to a (3,3)-connected honeycomb framework [15], as shown in figure 3(a). Rhombohedral anionic channels were formed through the above fourfold interpenetration of the anionic frameworks [figure 3(b)]. It presents the high fold-interpenetrating net constructed by only a single *btb* ligand. The channels are occupied by disordered DMF and  $\text{Me}_2\text{NH}_2$  cations. About 28.5% solvent-accessible volume is estimated using the PLATON software. The pores of the channels may be partly blocked by  $\text{Me}_2\text{NH}_2$  cations and DMA molecules, and the actual pore sizes are less than  $7.5 \times 7.5$  Å, and this was confirmed by the results of gas sorption measurements.

#### *[Mn<sub>3</sub>(btb)<sub>2</sub>(DMA)<sub>4</sub>·4DMA] (2)*

The asymmetric unit of **2** contains one and a half Mn(II) ions, one BTB anion, two coordinated DMA, and two free DMA molecules. As shown in figure 4, Mn1 adopts a distorted MnO<sub>6</sub> octahedral geometry and coordinated to four oxygens from three individual BTB<sup>3-</sup> and two oxygens from DMA molecules. The O1, O7, O3, and O4 atoms are the equatorial plane, and O5 and O8 occupy axial positions. Mn2 lies on an inversion center and is coordinated to six oxygens from six individual BTB ligands. A 2-D bilayer framework with large

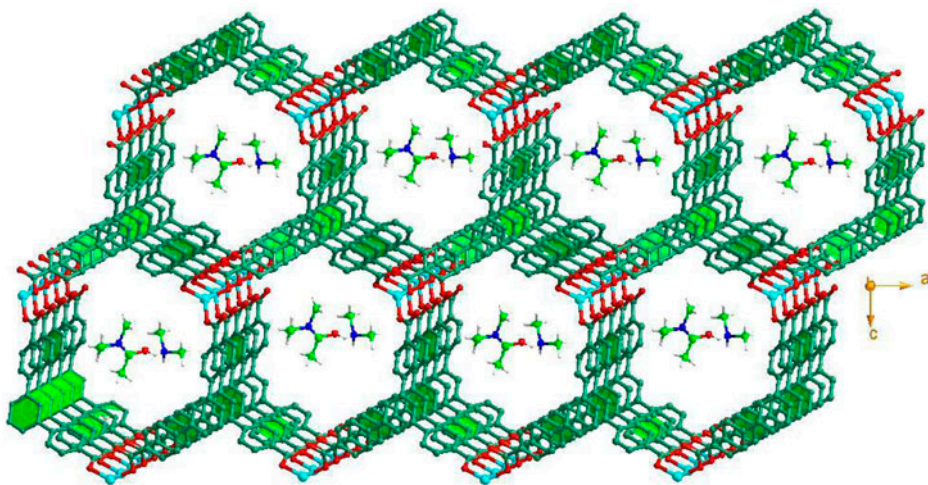


Figure 2. Perspective view of the 3-D net of the 1-D channel in **1**.

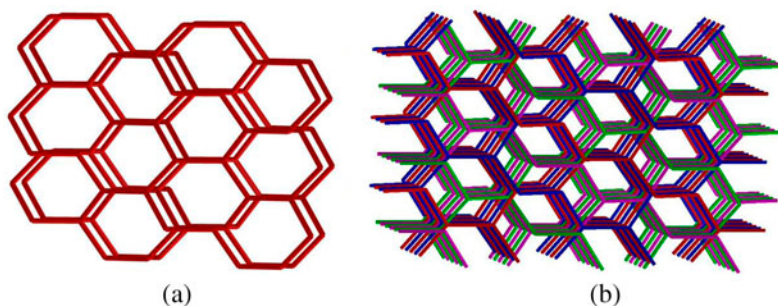


Figure 3. (a) View of the honeycomb topological net. (b) The topological structure of fourfold interpenetrated frameworks.

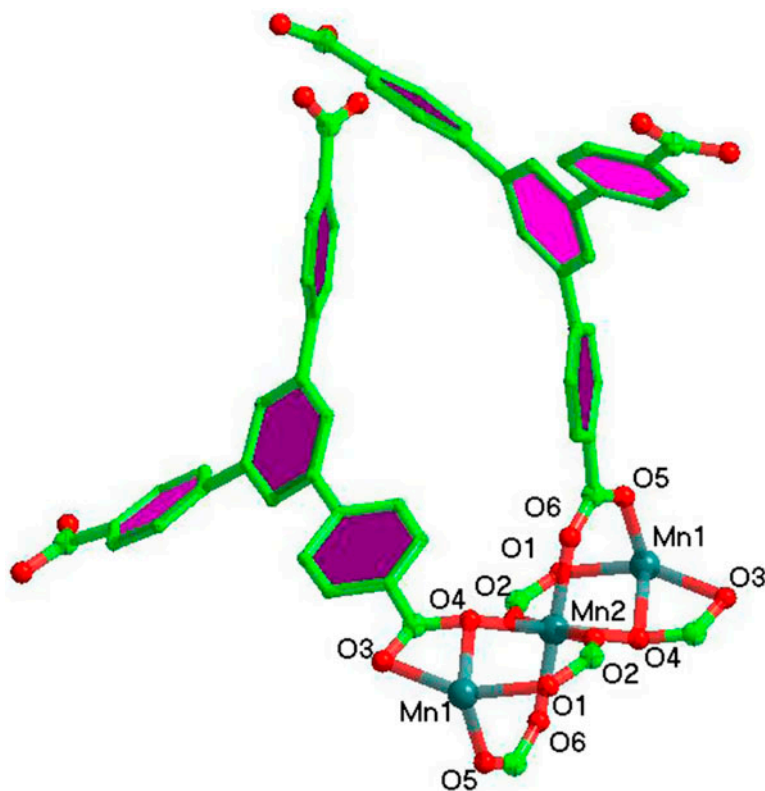


Figure 4. Coordination geometries of the metal centers and the ligand geometry in **2** (the two coordinated DMA molecules attached to Mn1 are omitted for clarity).

cavities is formed through the bridging BTB<sup>3-</sup> ligands (figure 5), and the cavities are occupied by guest DMA molecules. The cavities are blocked by the adjacent bilayer to make the 3-D structure almost nonporous. The structure of **2** is similar to the recently reported structures of polymers  $\{[\text{Cd}_3(\text{BTB})_2(\text{DEF})_4] \cdot 3\text{DEF}\}_n$  and  $\{[\text{Cd}_3(\text{BTB})_2(\text{DMF})_4] \cdot 3\text{DMF}\}_n$

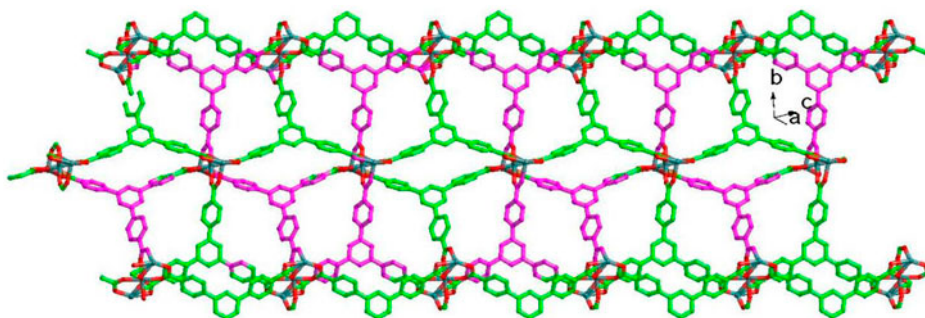


Figure 5. The honeycomb-like bilayer framework with large cavity (the guest DMA molecules in the cavities are omitted for clarity).

[12(b–c)]. The minor difference can be attributed to the bridged modes of the guest DMA/DMF/DEF molecules, which then induce the final coordination of  $\text{BTB}^{3-}$  in these polymers. A new polymer of  $[\text{Co}_3(\text{BTB})_2(\text{DMA})_4]_n$  with a linear trinuclear cobalt carboxylate cluster was prepared under  $100\text{ }^\circ\text{C}$  [15(d)] which also shows a 2-D layered structure of a 3,6-connected *kgd*-like net. The compound also takes significant sorption hysteresis for adsorbates with relatively strong interactions with the framework, such as  $\text{N}_2$  and  $\text{CO}_2$  [15(d)].

From the topological view, the structural feature is the presence of a new (3,6)-connected topology in **1**. The trinuclear cluster of the whole framework can be taken as 6-connected nodes, and  $\text{BTB}^{3-}$  can be viewed as 3-connected nodes (figure 6).

### FTIR, TGA, and XRPD

The asymmetric stretch  $\nu(\text{COO}^-)$  is at  $1617\text{ cm}^{-1}$  for **1**, and the symmetric stretch  $\nu(\text{COO}^-)$  is observed around  $1352\text{ cm}^{-1}$  for **1**. Thus, the order of the asymmetric and symmetric stretches,  $\Delta\nu_{\text{as}(\text{COO}^-)-\nu_{\text{s}}(\text{COO}^-)}$ , is more than  $200\text{ cm}^{-1}$ , indicating that carboxyl groups are coordinated monodentate to the metal [15(b)], consistent with the observed X-ray crystal structure of **1**. For **2**, the order of the asymmetric and symmetric stretches,  $\Delta\nu_{\text{as}(\text{COO}^-)-\nu_{\text{s}}(\text{COO}^-)}$ , is less than  $150\text{ cm}^{-1}$ , indicating that carboxyl groups are coordinated bidentate to the metal [15(b)], consistent with the observed X-ray crystal structure of **2**.

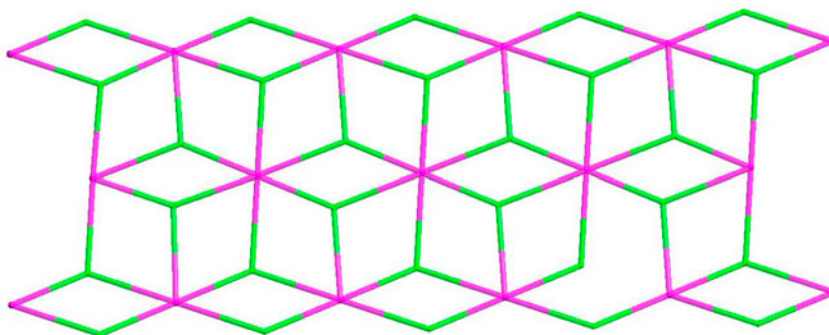


Figure 6. The topological structure of **2** (color code for the balls: Mn, pink; BTB node, green) (see <http://dx.doi.org/10.1080/00958972.2014.981168> for color version).



To study the stability of the polymer, TGA of **1** were performed (figure S1, see online supplemental material at <http://dx.doi.org/10.1080/00958972.2014.981168>). Compound **1** shows two weight loss steps. The first weight loss began at 60 °C and was completed at 226 °C. The observed weight loss of 31.1% corresponds to loss of the free and coordinated DMA molecules and Me<sub>2</sub>NH<sub>2</sub> (calcd: 30.5%). The second weight loss occurs from 305 to 805 °C, which can be attributed to elimination of btb. The 17.8% mass remnant at 890 °C is consistent with ZnO (19.1%). Compound **2** shows three weight loss steps. The first of 19.8% between 20 and 169 °C corresponds to release of four DMA molecules per formula unit (calcd: 20.1%). The second weight loss of 18.9% between 169 and 289 °C corresponds to release of four coordinated DMA molecules per formula unit (calcd: 20.1%), and the complex starts decomposing at 300 °C. The third deposition finishes at 750 °C, attributed to elimination of organic ligands (calcd: 69.8%).

To confirm the phase purity, original samples of **1** and **2** were characterized by XRPD at room temperature. The pattern that was simulated from the single-crystal X-ray data was in agreement with that observed, as shown in figure S2.

### Gas sorption

In order to check the permanent porosity of **1**, gas adsorption studies have been performed, as shown in figure 7. The activated sample of **1'** was prepared by keeping as-synthesized **1** in DMA for 1 day while refreshing the solvent twice during soaking and then vacuum drying at 120 °C overnight. The activated **1** has been studied for N<sub>2</sub> and H<sub>2</sub> at 77 K. The H<sub>2</sub> and N<sub>2</sub> sorption amounts rise gradually from  $P/P_0 = 0$  to 1.0. Both isotherms present typical Type-I curves and are characteristic of a microporous material [16]. Usually, this sorption feature can be attributed to some reasons. First, **1** is a 3-D interpenetrating structure and the void is occupied by the fourfold nets; second, the interaction between gas molecules and the full framework is very weak; and third, **1** is an anionic framework, thus, the pore may be blocked by the large and immovable [NH<sub>2</sub>(CH<sub>3</sub>)<sub>2</sub>]<sup>+</sup> cations. Despite **1** holding an apparent solvent accessible volume ratio of ca. 32% (estimated by PLATON considering only the solvent molecules) [17], it has no significant adsorption for N<sub>2</sub> and H<sub>2</sub> gas upon desolvation by long-time thermal activation under vacuum or after exchanging the higher boiling guest (DMA and H<sub>2</sub>O) with lower boiling molecule (MeOH and CH<sub>2</sub>Cl<sub>2</sub>) by

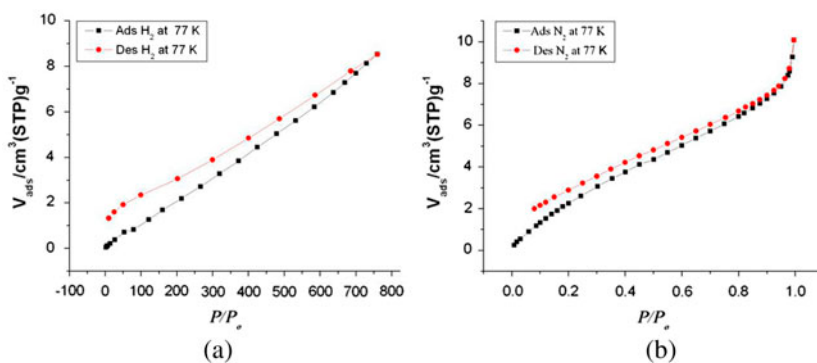


Figure 7. (a) Gas sorption isotherms at 77 K for H<sub>2</sub> in **1**. (b) Gas sorption isotherms at 77 K for N<sub>2</sub> in **1**.

soaking before degassing at room temperature under vacuum. This indicates that the channels are clogged by the large immovable  $\text{Me}_2\text{NH}_2^+$  cations. This gas sorption behavior has been observed at other alkylammonium@Zn-carboxylate polymers [18].

### Magnetism

The  $\chi_M T$  value per trinuclear manganese(II) unit was  $13.2 \text{ cm}^3 \text{ K M}^{-1}$  at 300 K (figure 8), indicating that all the manganese(II) ions are in the high-spin state. When decreasing the temperature, the  $\chi_M T$  decreases gradually and reaches a minimum ( $4.5 \text{ cm}^3 \text{ K M}^{-1}$ ) at 2 K. The variable-temperature magnetic susceptibility data of  $\text{Mn}^{\text{II}}$  trimmers were fitted according to the equation as follows [19]:

$$H = -J(S_{A1} \cdot S_B + S_{A2} \cdot S_B) - J'S_{A1} \cdot S_{A2}$$

$$S' = S_{A1} + S_{A2}$$

$$S = S' + S_B$$

$$E(S, S') = -\frac{J}{2}S(S+1) - \frac{J'-J}{2}(S'+1)$$

$$\chi = \frac{N\beta^2}{3kT} \frac{\sum_{S'=0}^{2S_A} \sum_{S=|S'-S_B|}^{S'+S_B} g_{S,S'}^2 S(S+1)(2S+1) \exp\left[-\frac{E(S,S')}{kT}\right]}{\sum_{S'=0}^{2S_A} \sum_{S=|S'-S_B|}^{S'+S_B} (2S+1) \exp\left[-\frac{E(S,S')}{kT}\right]} + TIP$$

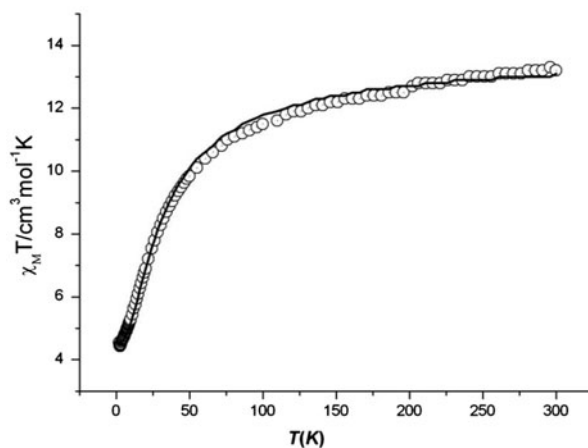


Figure 8. Plots  $\chi_M T$  vs.  $T$  for **2**; solid lines represent fits to the data.

$$S_A = S_B = \frac{5}{2}$$

$$J' = 0$$

$$g_{s,s'} = g$$

The best-fitting parameters are obtained as  $J = -2.73 \text{ cm}^{-1}$ ,  $g = 2.05$ , and  $TIP = 0 \text{ cm}^3 \text{ K M}^{-1}$ , indicating an anti-ferromagnetic interaction between adjacent manganese(II) ions. These values confirm the presence of anti-ferromagnetic interaction between the  $\text{Mn}^{2+}$  ions within a trinuclear subunit. The parameter  $\Phi_{\text{bend}}$  of the  $\text{Mn-O-C-O-Mn}$  is very important; larger  $\Phi_{\text{bend}}$  could generate a larger decrease in  $-J$  because of reduced overlap of the  $d_{x^2-y^2}$  orbital with the  $2p_x$  carboxylate oxygen orbital in the symmetric HOMO [20]. In the case of **1**, the  $\Phi_{\text{bend}}$  is 4.8, which is slightly smaller than that of  $[\text{Mn}_3(\text{L})(\text{DMA})\cdot 2\text{DMA}]$  ( $\text{H}_6\text{L} = \text{hexa}[4\text{-}(\text{carboxyphenyl})\text{oxamethyl}]\text{-3-oxapentane acid}$ ) [21]. A trinuclear Mn(II) compound of  $[\text{Mn}_3(\text{Hbptc})_2(2,2'\text{-bpy})_3(\text{H}_2\text{O})_8]\cdot 2\text{H}_2\text{O}$  ( $\text{H}_4\text{bptc} = \text{iphenyl-2,5,2',5'-tetracarboxylic acid}$ ,  $2,2'\text{-bpy} = 2,2'\text{-bipyridine}$ ) exhibits weak anti-ferromagnetic interaction. The authors infer that the small Weiss value is indicative of weak anti-ferromagnetic interactions between neighboring Mn(II) ions, possibly due to a long  $\text{Mn}\cdots\text{Mn}$  distance of  $6.801 \text{ \AA}$  [22].

### Luminescence

Organic-inorganic coordination polymers, especially those with  $d^{10}$  metal centers, have been investigated for their fluorescent properties and potential applications as fluorescence-emitting

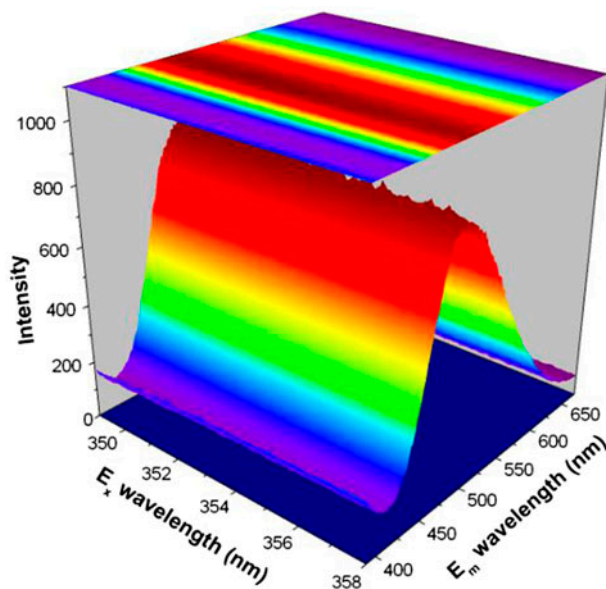


Figure 9. View of the 3-D luminescence at room temperature for **1**.

materials, such as light-emitting diodes [23, 24]. Therefore, **1** was studied in the solid state at room temperature (figure 9). Free H<sub>3</sub>btb shows an emission at 400 nm [25], while **1** shows the maximum emission peak at 528 nm ( $\lambda_{\text{em}} = 355$  nm). The luminescent lifetime is 5.87 ns for **1** (figure S3), a little longer than that of H<sub>3</sub>btb [25]. The formation of two types of excimeric sites is demonstrated for free btb in the solid state. The author also assumed that cyclic O–H···O bonds greatly facilitated the formation of low-energy excimers in free H<sub>3</sub>btb [25].

## Conclusion

We have synthesized two new polymers with different topological nets. The H<sub>2</sub> and N<sub>2</sub> gas sorption studies indicate that the channels may be clogged by the large and immovable Me<sub>2</sub>NH<sub>2</sub><sup>+</sup> cations and interpenetrated mode in **1**. Compound **1** exhibits strong photoluminescence at room temperature and may be suitable as a candidate as a luminescent material. The magnetic behavior of **2** shows the presence of anti-ferromagnetic interaction between the Mn<sup>2+</sup> ions within a trinuclear subunit.

## Funding

This work was partially supported by the Grants from Sichuan University of Science and Engineering; the Institute of Functionalized Materials [grant number 2012KY12], [grant number 2014PY01]; the Opening Project of Key Laboratory of Green Catalysis of Sichuan Institutes of High Education [grant number LYJ1207]; and the Education Committee of Sichuan Province [grant number 12ZA090], [grant number 13ZB0131], and [grant number 14ZB0220].

## References

- [1] S.T. Bramwell, M.J.P. Gingras. *Science*, **294**, 1495 (2001).
- [2] M. Eddaoudi, D.B. Moler, H.-L. Li, B.-L. Chen, T.M. Reineke, M. O’Keeffe, O.M. Yaghi. *Acc. Chem. Res.*, **34**, 319 (2001).
- [3] R. Ganguly, B. Sreenivasulu, J.J. Vittal. *Coord. Chem. Rev.*, **252**, 1027 (2008).
- [4] J.-P. Zhang, Y.-Y. Lin, X.-C. Huang, X.-M. Chen. *J. Am. Chem. Soc.*, **127**, 5495 (2009).
- [5] O.K. Farha, C.D. Malliakas, M.G. Kanatzidis, J.T. Hupp. *J. Am. Chem. Soc.*, **132**, 950 (2009).
- [6] J.-R. Li, J. Sculley, H.-C. Zhou. *Chem. Rev.*, **112**, 869 (2011).
- [7] Z.Q. Wang, V.C. Kravtsov, M.J. Zaworotko. *Angew. Chem. Int. Ed.*, **41**, 2821 (2005).
- [8] J.S. Seo, D. Whang, H. Lee, S.I. Jun, J. Oh, Y.J. Jeon, K. Kim. *Nature*, **404**, 982 (2000).
- [9] (a) H. Xiang, W.Y. Gao, D.C. Zhong, L. Jiang, T.B. Lu. *CrystEngComm*, **13**, 5825 (2011); (b) M. Kim, J.A. Boissonnault, C.A. Allen, P.V. Dau, S.M. Cohen. *Dalton Trans.*, **41**, 6277 (2012); (c) Q.X. Yao, J.L. Sun, K. Li, J. Su, M.V. Peskov, X.D. Zou. *Dalton Trans.*, **41**, 3953 (2012); (d) S.R. Caskey, A.J. Matzger. *Inorg. Chem.*, **47**, 7942 (2008); (e) L. Hou, J.P. Zhang, X.M. Chen. *Cryst. Growth Des.*, **9**, 2415 (2009); (f) Z.Q. Wang, K.K. Tanabe, S.M. Cohen. *Inorg. Chem.*, **48**, 296 (2009); (g) N. Klein, I. Senkowska, I.A. Baburin, R. Grunker, U. Stoeck, M. Schlichtenmayer, B. Streppel, U. Mueller, S. Leoni, M. Hirscher, S. Kaskel. *Chem.-Eur. J.*, **17**, 13007 (2011).
- [10] X.R. Hao, X.L. Wang, K.Z. Shao, G.S. Yang, Z.M. Su, G. Yuan. *CrystEngComm*, **14**, 5596 (2012).
- [11] N. Klein, I. Senkowska, K. Gedrich, U. Stoeck, A. Henschel, U. Mueller, S. Kaskel. *Angew. Chem. Int. Ed.*, **48**, 9954 (2009).
- [12] (a) R. Heck, J. Bacsu, J.E. Warren, M.J. Rosseinsky, D. Bradshaw. *CrystEngComm*, **10**, 1687 (2008); (b) J. Kim, B. Chen, T.M. Reineke, H. Li, M. Eddaoudi, D.B. Moler, M. O’Keeffe, O.M. Yaghi. *J. Am. Chem. Soc.*, **123**, 8239 (2001); (c) H. Xiang, W.Y. Gao, D.C. Zhong, L. Jiang, T.B. Lu. *CrystEngComm*, **13**, 5825 (2011).
- [13] G.M. Sheldrick. *SHELXL-97: Program for Structure Determination and Refinement*, University of Göttingen, Göttingen (1997).
- [14] G.M. Sheldrick. *Acta Cryst.*, **A**, **64**, 112 (2008).
- [15] (a) V.A. Blatov, D.M. Proserpio. *Acta Crystallogr., Sect. A: Found Crystallogr.*, **65**, 202 (2009); (b) K. Nakamoto, *Infrared and Raman Spectra of Inorganic and Coordination Compounds*, 5th Edn, Wiley Interscience, New York, NY (1997); (c) D.W. Kim, X.K. Song, J.H. Yoon, M.S. Lah. *Cryst. Growth Des.*, **12**, 4186 (2012); (d) Y.L. Huang, Y.N. Gong, L. Jiang, T.B. Lu. *Chem. Commun.*, **49**, 1753 (2013).

- [16] (a) X.R. Hao, X.L. Wang, Z.M. Su, K.Z. Shao, Y.H. Zhao, Y.Q. Lan, Y.M. Fu. *Dalton Trans.*, 8562, (2009); (b) D.-C. Zhong, W.-X. Zhang, F.-L. Cao, L. Jiang, T.-B. Lu. *Chem. Commun.*, **47**, 1204 (2011); F. Rouquerol, J. Rouquerol, K. Sing. *Adsorption by Powders and Porous Solids.*, Academic Press, London (1999); (c) J.-R. Li, Y. Tao, Q. Yu, X.-H. Bu, H. Sakamoto, S. Kitagawa. *Chem.-Eur. J.*, **14**, 2771 (2008); (d) M. Xue, Z.-J. Zhang, S.-C. Xiang, Z. Jin, C.-D. Liang, G.-S. Zhu, S.-L. Qiu, B.-L. Chen. *J. Mater. Chem.*, **20**, 3984 (2010).
- [17] A.L. Spek. *J. Appl. Crystallogr.*, **36**, 7 (2003).
- [18] (a) X.F. Wang, Y.B. Zhang, X.N. Cheng, X.M. Chen. *CrystEngComm*, **10**, 753 (2008); (b) M.W. Zhang, M. Bosch, T. Gentile III, H.C. Zhou. *Cryst. Eng. Comm.*, **16**, 4069 (2014); (c) S.-T. Zheng, J.J. Bu, W. Tao, C. Chou, P.-Y. Feng, X.-H. Bu. *Angew. Chem., Int. Ed.*, **50**, 8858 (2011); (d) J.F. Eubank, H. Mouttaki, A.J. Cairns, Y. Belmabkhout, L. Wojtas, R. Luebke, M. Alkordi, M. Eddaoudi. *J. Am. Chem. Soc.*, **133**, 14204 (2011); (e) Y.-Y. Liu, J.-F. Ma, J. Yang, Z.-M. Su. *Inorg. Chem.*, **46**, 3027 (2007); (f) D.F. Sun, Y.X. Ke, D.J. Collins, G.A. Lorigan, H.C. Zhou. *Inorg. Chem.*, **46**, 2725 (2007); (g) L.H. Xie, J.B. Lin, X.M. Liu, W. Xue, W.X. Zhang, S.X. Liu, J.P. Zhang, X.M. Chen. *Sci. Chin. Chem.*, **53**, 2144 (2010).
- [19] K. Olivier, *Inorganic Chemistry*, VCH, New York (1993).
- [20] J.L. Manson, E. Ressouche, J.S. Miller. *Inorg. Chem.*, **39**, 1135 (2000).
- [21] A.D. Burrows, C.G. Frost, M.F. Mahon, M. Winsper, C. Richardson, J.P. Attfield, J.A. Rodgers. *Dalton Trans.*, 6788 (2008).
- [22] Y.Y. Wang, Q.H. Liu, W. Wei, H. Du, J.M. Shi, Y.Q. Zhang. *J. Coord. Chem.*, **66**, 254 (2013).
- [23] D.-C. Zhong, W.-G. Lu, L. Jiang, X.-L. Feng, T.-B. Lu. *Cryst. Growth Des.*, **10**, 739 (2010).
- [24] D.F. Sava, L.E.S. Rohwer, M.A. Rodriguez, T.M. Nenoff. *J. Am. Chem. Soc.*, **134**, 3983 (2012).
- [25] V. Vergadou, G. Pistolis, A. Michaelides, G. Varvounis, M. Siskos, N. Boukos, S. Skoulika. *Cryst. Growth Des.*, **6**, 2486 (2006).